Chinese Chemical Letters 31 (2020) 635–642

Contents lists available at ScienceDirect

Chinese Chemical Letters

journal homepage: www.elsevier.com/locate/cclet

Review

Metal-organic frameworks and their derivatives for Li–air batteries

Yu Dong, Siwu Li, Shanshan Hong, Lu Wang*, Bo Wang*

Beijing Key Laboratory of Photoelectronic/Electrophotonic Conversion Materials, Key Laboratory of Cluster Science, Ministry of Education, School of Chemistry and Chemical Engineering, Beijing Institute of Technology, Beijing 100081, China

ARTICLE INFO

Article history:
Received 1 May 2019
Received in revised form 17 June 2019
Accepted 15 August 2019
Available online 7 September 2019

Keywords:
Metal-organic frameworks
MOF-derived materials
Li–air batteries
Li–O_2 batteries
Li–CO_2 batteries

ABSTRACT

Metal-organic frameworks (MOFs) are a class of outstanding materials in Li–air batteries because of their high surface areas, tailorable pore sizes and diverse catalytic centers. However, MOF-based batteries are facing challenges such as poor electronic conductivity and inferior long-cycle stability that limit their further development. This review first summarizes the progress of pristine MOFs and MOF-derived materials in Li–air batteries in the past 5 years, then provides a perspective for subsequent development of MOFs and their derivatives in this emerging field.

1. Introduction

Rechargeable non-aqueous metal-air batteries are viewed as potential candidates to surpass Li–ion batteries for next-generation electrochemical energy storage systems [1–4]. Particularly, Li–air batteries (LABs) have attracted worldwide attention owing to the predominant theoretical gravimetric energy density of 3500 Wh/kg [5–8].

The ideal operating environment of practical LABs is ambient air, in which oxygen is the main contributing gas. However, the components of air are extremely complex (including H_2O, CO_2, CO, N_2, *etc.*). To avoid unnecessary parasitic reactions, nowadays most experiments employed pure and dry oxygen instead of air [8]. In this case, LABs tested in O_2 are often known as Li–O_2 batteries (LOBs).

Metal-organic frameworks (MOFs) are a class of functional porous crystal materials which are self-assembled by metal ions/clusters and various organic ligands. MOFs possess high specific surface area, tunable pore sizes and abundant catalytic sites, which have been widely and deeply studied in gas capture, separation and catalysis [9–18]. Furthermore, MOF-derived porous materials have also attracted wide attention in the past decades. The various options of metals and ligands in MOFs provide rich sources and solid foundations for the design and fine-tune.

To elucidate the recent development of MOF-based porous materials in LABs, the progress can be categorized into two sections in terms of the composition of catalysts: 1) pristine MOFs in Li–O_2/CO_2/air batteries, 2) MOF-derived materials included metal, metal oxides, carbides, nitrides, sulfides and metal-free materials in Li–O_2/CO_2 batteries.

2. Pristine MOFs for Li–air batteries

The comprehensive utilization of pristine MOFs in the field of LABs has emerged in recent years, mainly as gaseous catalysts, separators and O_2-diffusion membranes.

The advantages of MOFs include high specific surface area, strong gas enrichment ability and open metal sites, while the disadvantage is low electrical conductivity. The charge transfer efficiency in MOFs should be improved. Among all MOF-based cells, Mn element may be a kind of promising metal source of catalysts in LABs. For example, Mn-MOF-74 and $Mn(HCOO)_2$, they showed excellent performance in their corresponding systems.

2.1. Cathode catalysts in Li–O_2 batteries

For the first time, Li's group synthesized five pristine-MOF-based electrodes and explored their performance in LOBs (Fig. 1a) [19]. The cathode with catalytic open metal centers and porous frameworks exhibited predominant effects in the promotion of discharge capacity (Fig. 1b). MOF-5, the one without open metal sites showed the lowest O_2 uptake among all MOFs investigated. Inversely, Mn_2(DOBDC) (DOBDC = 2,5-dioxide-1,4-benzenedicarboxylate) with one-dimensional channels and immense O_2 adsorption capability exhibited the best performance among five MOFs. The capacity performance of Mn_2(DOBDC) reaches 9420 mAh/g, three

* Corresponding authors.
E-mail addresses: luwang@bit.edu.cn (L. Wang), bowang@bit.edu.cn (B. Wang).

https://doi.org/10.1016/j.cclet.2019.08.021

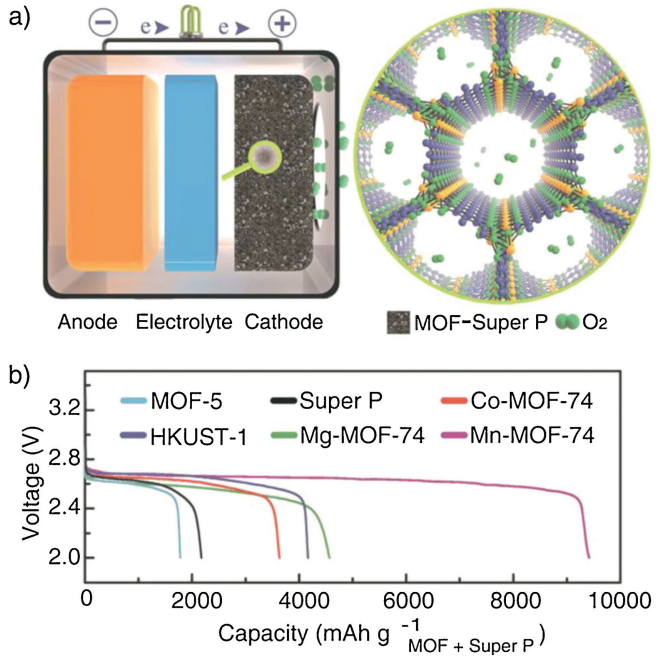

Fig. 1. (a) Schematic illustration of a Li-O_2 cell using MOF–Super P composite as the O_2 electrode. Oxygen molecules relative sizes reduced for clarity. (b) Discharge profiles of the Li-O_2 cells using MOF–Super P composites or Super P only under O_2 atmosphere with a current of 50 mA/g at room temperature. Reprinted with permission [19]. Copyright 2014, Wiley-VCH.

times higher than that of Super-P (2170 mAh/g) at a current density of 50 mA/g. Beyond Super-P, the authors also highlighted the advantages of open sites with $Mn_2(DOBDC)(H_2O)_2$, a control group that occupies catalytic open sites. The coin-type cell based on $Mn_2(DOBDC)(H_2O)_2$ just showed the discharge capacity of 2820 mA h/g. In order to verify whether the increase capacity was contributed by side reactions, the authors characterized the gas products during the battery charging process with the help of DEMS (differential electrochemical mass spectrometry) test. DEMS results showed that the products were almost pure oxygen, which reflected MOF did not catalyze side reactions of the battery, including the decomposition of electrolyte.

In addition, Ni-MOFs are also potential catalysts in LOBs. A micro-nano structural Ni-MOF was reported by Chen's group [20]. Ni(4,4′-bipy)(H_3BTC) (4,4′-bipy = 4,4′-bipyridine; H_3BTC = 1,3,5-benzenetricarboxylic acid), was a high-performance bifunctional oxygen catalyst owing to its 3D unique architecture of micro-channels and nanopores (Fig. 2). As a result, the full discharge capacity of 9000 mAh/g was achieved at the area current density of 0.12 mA/cm^2, and a high columbic efficiency of 80% with a cut-off capacity of 600 mA/g was shown at 0.6 mA/cm^2. Besides, the terminal discharge/charge plateau is steady during 170 cycles. Surprisingly, a specific energy density of ~478 Wh/kg was launched during the primary discharge by the "plastic reversible Li–O_2 batteries". This study not only indirectly observed the phenomenon of depositing discharge products in the holes of MOFs by SEM (scanning electron microscopy) in fundamental part, but also made a breakthrough in technological value.

The poor electron transport in MOFs skeletons usually hampers their performance in electrochemical fields. Therefore, it is imperative to enhance the conductivity of MOFs. Nanosized Co-MOF-74 was synthesized in Li's group in their later study [21]. Owing to the detects in nano-crystals, the cathodic catalyst provided more abundant active sites. At the current density of 100 mA/g, the discharge capacity of Co-MOF-74 was 11,350 mAh/g and the rate capability was enhanced. Therefore, downsizing MOFs particles into nanorods is an effective strategy to obtain uniform morphologies that can provide a faster charge-transport route and promote the activity of oxygen reactants.

Moreover, another pathway to improve the conductivity is to synthesize extremely thin 2D nanosheets. 2D M-BDC nanosheets (M = Mn/Co/Ni, BDC = 1,4-benzenedicarboxylate) expose more metal active sites, yielding closer contact with electrolyte and oxygen, and faster ions and charges transfer [22]. Among them, 2D Mn-MOF, as the best performer, displayed an initial discharge capacity of 9469 mAh/g and retained more than 200 cycles at 100 mA/g. It was ascribed to the fact that 2D Mn-MOFs based cathode made full use of open metal sites and ultrahigh specific surface areas, guaranteeing an outstanding discharge capacity. Remarkably, Mn-O clusters also strengthen the electrocatalytic activity of the electrode in the oxygen evolution reaction.

Subsequently, in comparison with synthesizing nano-MOFs and nanosheets, the synergistic effect of multimetallic catalytic sites was also discussed as an approach to improve battery performance [23]. Lee's group utilized MnCo-MOF-74 as the cathode material, which delivers a discharge specific capacity of 11150 mAh/g at the current density of 200 mA/g. Besides, compared to Mn-MOF-74, the discharge products of Li_2O_2 and LiOH can be fully decomposed

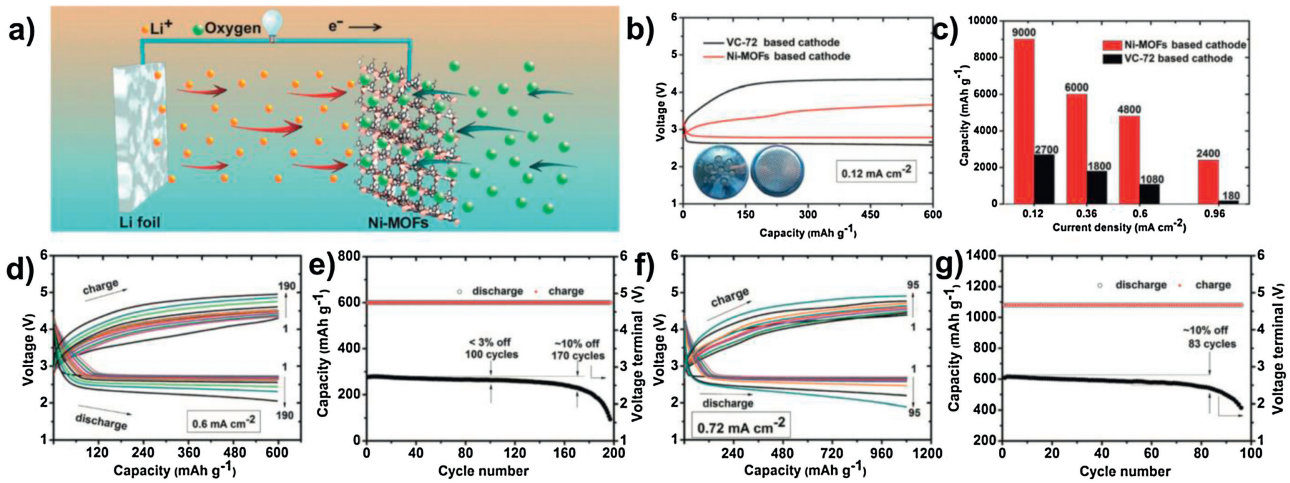

Fig. 2. (a) The scheme of Ni-MOFs-based Li-O_2 battery. (b–g) Electrochemical performance of Ni-MOFs-based Li-O_2. Reprinted with permission [20]. Copyright 2015, The Royal Society of Chemistry.

on MnCo-MOF-74 based electrode according to PXRD (powder X-ray diffraction) test, demonstrating that the reversibility and efficiency of the LOBs can be improved by the bifunctional catalyst.

2.2. Separator in Li–O_2 batteries

MOFs also play another important role in the Li–O_2 system. The strategy of dual redox mediators (RM), such as DBBQ (DBBQ = 2,5-di-*tert*-butyl-1,4-benzoquinone) and TTF^+ (TTF = tetrathiafulvalene), can improve the activities of OER (oxygen evolution reaction) and ORR (oxygen reduction reaction). However, the shuttle effect of RM between cathode and anode causes severe Li degradation, thus affecting the lifespan of battery. Due to the tunable pores and channels, MOFs were investigated for separator application.

With uniform channels of HKUST-1, Zhou *et al.* synthesized *in situ* grown HKUST-1@Celgard separators [24]. Contrast with 22 cycles of commercial Celgard separator, the cell based on HKUST-1@Celgard separator exhibited excellent stability up to 100 cycles at a high current density of 1 A/g within a capacity limitation of 5000 mAh/g. As a Li^+ sieve, the flexible separator restrained the diffusion of RM, thereby preventing the erosion of Li anode and maximizing the benefit of RM strategy (Fig. 3). The flexible separator was also used to fabricate a pouch-type battery, which showed potential in large-scale energy storage applications.

2.3. O_2-diffusion membrane in Li–air batteries

Water vapor and CO_2 in ambient air seriously affect the cycle life of batteries, and O_2 selective membrane can effectively prevent them from entering the semi-open system of LABs. The application of controllable-pores MOFs in the O_2-diffusion membrane was also developed.

The hydrophobic membrane made with the combination of CAU-1-NH_2, PDA (polydopamine) and PMMA (polymethylmethacrylate) had magnificent thermal and electrochemical stability [25]. CO_2 and H_2O molecules were captured and prevented effectively by the multifunctional groups of —NH_2, —OH and —C=O. As a result, the oxygen-permeation membrane promoted the cycling performance from 7 cycles without MMM (mixed matrix membrane) to 66 cycles at 450 mA/g in LOBs under 30% relative humidity.

2.4. Cathode catalysts in Li–CO_2 batteries

With the deepening of LABs research, the multicomponent gas systems have been exploring, such as O_2 and CO_2 system with different volume ratio [26]. Then, Li–CO_2 batteries with Li_2CO_3 as the main discharge product are also developed. Li_2CO_3, the more stable discharge product of LABs than Li_2O_2 ($\Delta_fG^o(Li_2CO_3)$ = −1132.1 kJ/mol, $\Delta_fG^o(Li_2O_2)$ = −578.9 kJ/mol), exhibits overly high overpotential, deteriorating the cycling stability of the battery [27–30]. It is important not only to investigate the electrochemical process of formation and decomposition of Li_2CO_3, also to provide a new type of energy storage device for high concentrations of CO_2 circumstances (such as Mars, outer space exploration in the future) [28,29].

Our group firstly investigated the performance of eight kinds of materials, including porous MOFs and non-porous materials (MnO and $MnCO_3$) in the Li–CO_2 system (Fig. 4) [31]. Due to the high capability of CO_2 adsorption, Mn_2(DOBDC)-based electrocatalyst exhibited ultrahigh discharge specific capacity of 18022 mAh/g at 50 mA/g. Besides, $Mn(HCOO)_2$ showed lower charge potential (~4.0 V) at a high current density of 200 mA/g and kept 50 cycles. The reaction route was confirmed by Raman and DEMS. And MOFs promoted the electron transfer on the interface evidenced by SEM and EIS (electrochemical impedance spectroscopy). Q_{st}, which presents isosteric heats of adsorption, is another important factor to reveal the interaction between frameworks and CO_2 molecules. The Q_{st} of Mn_2(DOBDC) is higher than that of $Mn(HCOO)_2$, which means more efficient decomposition of Li_2CO_3 by $Mn(HCOO)_2$. And we found that $Mn(HCOO)_2$ exhibited lower charge overpotential at the higher current density of 200 mA/g.

In a word, pristine MOFs were investigated as cathode electrocatalysts, separators and oxygen-permeation membranes in LABs. As an oxygen-permeation membrane, it can repulse carbon dioxide and moisture. With the advantages of designable pore sizes, abundant catalytic sites and high gas adsorption capability of MOFs, the semi-open system of LABs can sustain better cycling performance and higher energy efficiency.

3. MOF-derived materials for Li–O_2/CO_2 batteries

It is generally accepted that transition metals and their oxides are effective electrocatalysts for OER and ORR. However, traditional fabrication methods usually lead to the agglomeration of particles inevitably. MOFs as precursors can provide homogeneously distributed catalytic sites, benefiting from their structural periodic arrangement of metal centers and organic linkers. Moreover, MOF-derived materials also possess large surface areas and promoted electrical conductivity taking advantage of the carbon coatings.

3.1. MOF-derived metal in Li–O_2 batteries

Among all transition metals, cobalt has been identified as favorable candidates. Recently, Wang's group reported Co nanoparticles derived from Co-MOF (2-methylimidazole as linker) with 3D-print self-standing architecture [32]. The printable ink was first mixed with Co-MOF powder and Pluronic F127. Then the shaped

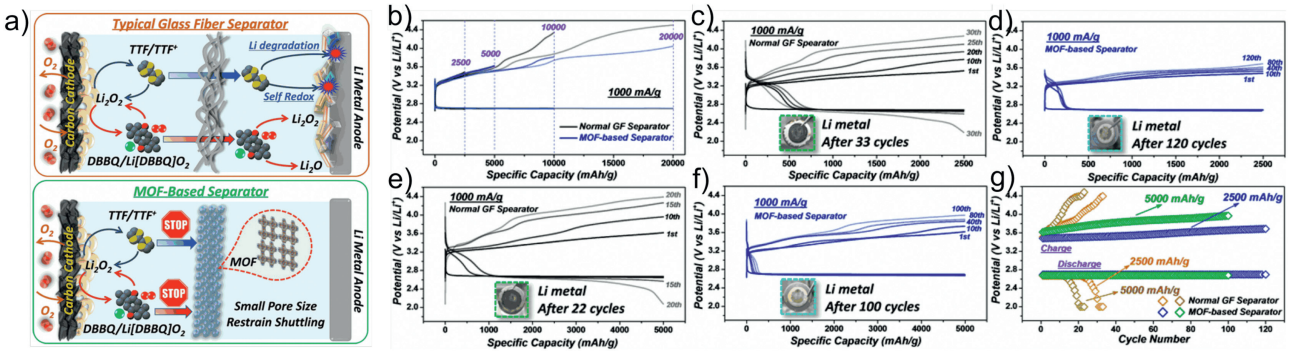

Fig. 3. (a) Schematic Illustrations of typical glass fiber separator and MOF-based separator with small pore size to restrain dual redox mediator (RM) shutting. (b–g) Electrochemical performance of Li–O_2 coin cells with RMs. Reprinted with permission [24]. Copyright 2018, American Chemical Society.

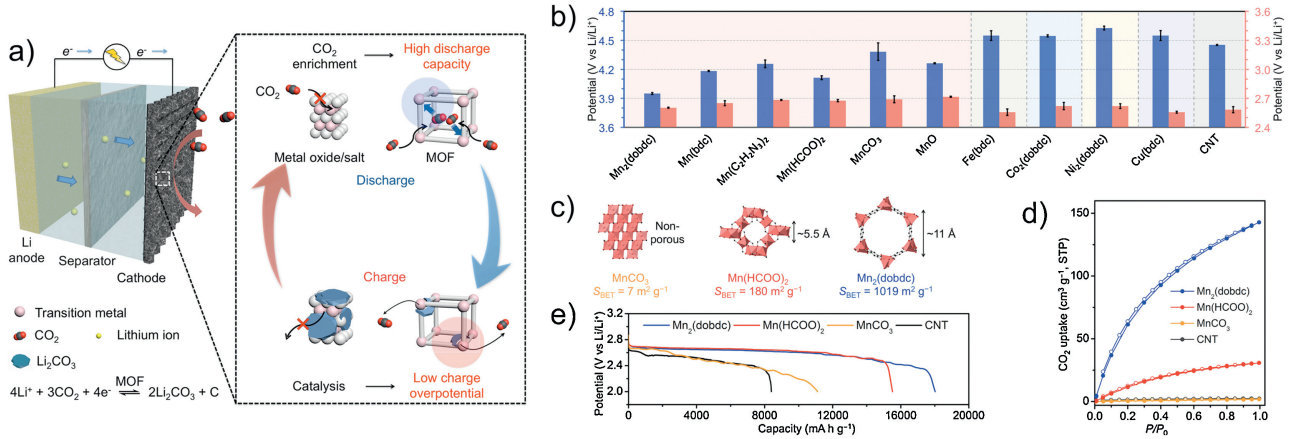

Fig. 4. (a) Scheme of the advantages of a Li-CO_2 battery equipped with a MOF-based CO_2 electrode. (b) Average discharge (red, right side) and charge (blue, left side) potentials of different electrodes upon operation at 50 mA/g with a capacity limit of 1000 mAh/g. (c) Crystal structures of $MnCO_3$, $Mn(HCOO)_2$ and Mn_2(DOBDC) along certain directions. (d) CO_2 adsorption isotherms at 298 K. (e) discharge voltage curves of Mn_2(DOBDC), $Mn(HCOO)_2$, $MnCO_3$ and CNTs at 50 mA/g with a cut-off voltage of 2.0 V. Reprinted with permission [31]. Copyright 2018, The Royal Society of Chemistry.

3D-print-Co-MOF was annealed into 3D-print-nitrogen carbon-Co frameworks (denoted as 3DP-NC-Co). In comparison with NC-Co powder only, 3DP-NC-Co had a higher specific surface area of 640 m^2/g. 3DP-NC-Co possess a porous conducting matrix and numerous micro- and mesopores flakes. Simultaneously, the conductivity of this self-supporting framework is about 2.2×10^3 S/m which extremely benefits the diffusion of oxygen/Li^+ and the reversibility of discharge products. As a result, the 3DP-NC-Co cathode delivered exceptional performance in non-aqueous LOBs. NC-Co powder casted on the carbon paper directly (denoted as RP-NC-Co) and NC-Co *in situ* grown on the carbon paper (denoted as CP-NC-Co) were employed respectively for comparison in this study. 3DP-NC-Co displayed superior discharge capacity (1124 mAh/$g_{electrode}$) than that of RP-NC-Co (109 mAh/$g_{electrode}$) and CP-NC-Co (99 mAh/$g_{electrode}$) based on the mass of the whole electrode at 0.05 mA/cm^2. However, according to the mass of NC-Co, the capacity of 3DP-NC-Co was lower than that of CP-NC-Co. Furthermore, lower overpotential and longer cycle life were obtained by 3DP-NC-Co cathode with a capacity-limit of 1 mAh/g at 0.1 mA/cm^2. Remarkably, the practical specific energy of cell attained 798 Wh/kg and showed a new perspective in the large-scale synthesis of cathode in practical LABs.

In addition to Co, Ru-element catalysts often show high catalytic activities in LOBs. Recently, Shao's group fabricated Ru-MOF [33]. By further calcining, they synthesized Ru-nanoparticle carbon composite (Ru-MOF–C). The batteries achieved ultra-long 800 cycles at current density of 500 mA/g. Moreover, they proposed a mechanism of regenerative surface to elucidate the excellent cycling performance.

Owing to the synergistic effect of different active metal sources, bimetallic MOFs as precursors have been studied widely [34–37]. The bimetal-alloy catalyst, FeCo/CNT composite, showed the advantages of mixed metal and core-shell structure [38]. After pyrolyzing the Fe/Co MOF in N_2 at 600 °C, the resulting catalyst with a core-shell structure was fabricated. Based on that, the catalytic performance of OER and ORR was investigated and a four-electron transfer path and a slight ΔE value of 0.79 V in alkaline aqueous solution were confirmed. The battery performance is considerable that it can run 40 cycles at limited capacity of 500 mAh/g at 100 mA/g and the gap between discharge and charge plateau was reduced to 1.55 V.

3.2. MOF-derived metal oxides in Li–O_2 batteries

MOF-derived Co_3O_4 composites stand out for their attractive electrocatalytic activities. Co_3O_4 with graphitic porous carbon was

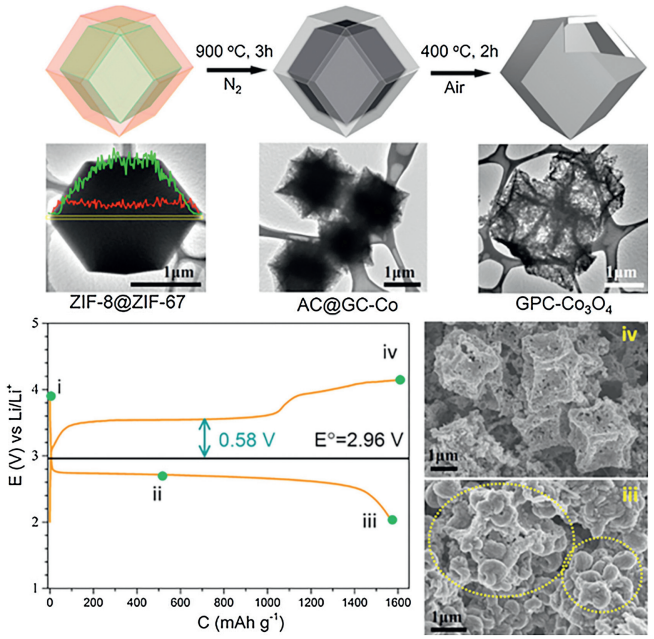

Fig. 5. Synthetic scheme and corresponding TEM images for the preparation of core-shell ZIF-8@ZIF-67 crystals, AC@GC-Co and GPC-Co_3O_4, and SEM images of the GPC-Co_3O_4 cathode after full discharge/charge of the Li–O_2 batteries. Reprinted with permission [39]. Copyright 2016, American Chemical Society.

fabricated *via* seed growth of ZIF-8@ZIF-67 polyhedron (Fig. 5). Yamauchi's group reported this core-shell graphitic porous carbon-Co_3O_4 (GPC-Co_3O_4) with mesoporous structure as the O_2 electrode [39]. GPC-Co_3O_4 achieved monodispersed catalytic active sites and sufficient electronic conductivity. As a result, the coin cell based on GPC-Co_3O_4 cathode delivered stable discharge/charge plateau with a voltage gap of 0.58 V between 2.7∼3.5 V. With the cut-off capacity set at 500 mAh/g, the cage-type electrode displayed attractive rate capability at 250, 375, 500 mA/g to 1250 mA/g. Compared to commercial Super P which can only perform 10 cycles, longer cycle life up to 50 cycles was obtained by GPC-Co_3O_4 with stable capacity at 250 mA/g.

Binder-free Co_3O_4/carbon fiber composite was synthesized to fabricate self-standing electrode in LOBs [40]. ZIF-9/PAN nanofiber, which worked as the precursor and was obtained by the electrospinning method, was calcined at 900 °C in the N_2

atmosphere and then oxidized at 280 °C under air. The prepared O_2 cathode possesses homogeneous catalytic metal sites and porous carbon. Compared to the pristine carbon nanofibers, 10 times higher full discharge capacity and longer cycle life at 500 mA/g were achieved by Co_3O_4/carbon nanofibers electrodes due to the high surface area and stable distribution. The rate performance of Co_3O_4/carbon nanofibers electrodes was further explored and kept the same cyclic life at a higher current density of 800 mA/g.

Sun's group explored a self-standing cathode of Co-ZIF-67 derivative with modified wood (Wood-D/Co_3O_4/C) which possess unique reaction interface, hierarchical pore structures and ultra-fast mass transport [41]. Wood/Co_3O_4/C based electrode showed an impressive reversibility of more than 380 cycles at 1.0 mA/cm^2 by curtailing the capacity to 1 mAh/cm^2. In comparison with Co_3O_4/C at Ni foam prepared by rolling-paste, wood-D/Co_3O_4/C possesses split-up transfer of Li^+/O_2 and its architecture of abundant vertical tubes helps the homogeneous growth of discharge products. Furthermore, they found that the capacitive contribution is around 35% of total capacity by cyclic voltammetry and demonstrated that capacitive contribution helps to promote capacity and reversibility.

What is more, cobalt-N-doped carbon system displayed their potential to enhance ORR activity. Yu's group designed a ZIF-9 derivative named Co-CoO@NC with disk-type homogeneous cobalt nanoparticles [42]. The bridge bonds of Co-N-C and ample oxygen vacancies enhance not only electrical conductivity but also activities of ORR. As a result, its initial discharge capacity showed 5582 mAh/g at 0.05 mA/cm^2. In contrast with KB, the O_2 electrode based on Co-CoO@NC not only exhibits much higher rate performance but also better cycle life.

Hierarchical architecture including macropores and micropores can accommodate plentiful reaction products. In view of this, Bu's group synthesized CNF@Co-CoO (CNF = carbon nano fibers) derived from PAN@ZIF-67 (PAN = polyacrylonitrile) [43]. The feature of unique "gypsophila-like" morphology and *in situ* synthetic route improved the reversibility of the cell which the CNF@Co-CoO cathode showed a longer lifespan of 38 cycles with a capacity-limit of 500 mAh/g at 200 mA/g as compared to pure CNF. What's more, the architecture enabled the cell to exhibit the good initial full discharge-charge capacity of 3500 mAh/g at 200 mA/g and coulombic efficiency of 73.7%, respectively.

Comparably, the similar 3D hierarchical structure was studied in Yin's group [44]. After *in situ* solvothermal treatment on nickel foam and a pyrolysis process, Co/CoO/C@Ni nanocomposite with mesoporous and microsheets was obtained, exhibiting promising bifunctional electrocatalytic performance in LOBs. The higher discharge and lower charge overpotential about 0.5 V were obtained, surpassing that of Super P with a cut-off capacity of 2000 mAh/g. Besides, Co/CoO/C@Ni displayed better cycle life (70 cycles) and rate capability. The specific discharge-charge capacity at various current densities of Co/CoO/C@Ni electrode was obviously higher than that of Super P. Remarkably, the highest capacity based on Co/CoO/C@Ni was 8000 mAh/g at the current density of 0.1 mA/cm^2.

Other metal oxides were also developed. In early studies, γ-Fe_2O_3 pyrolyzed from MIL-100(Fe) and Cr_2O_3 derived from MIL–101(Cr) were investigated [45,46].

As for bimetallic oxides, the hierarchical nanocages of ZnO/$ZnFe_2O_4$/C (ZZFC) derived from Fe(III)-MOF-5 were demonstrated to be effective in high performance in LOBs according to an earlier study [47]. The electrode with ZZFC exhibited an ultrahigh discharge capacity up to over 11000 mAh/g at 300 mA/g, and showed a higher reversibility of 15 cycles with the improved limited capacity of 5000 mAh/g.

Spinel oxides as electrode materials are extensively employed in energy storage applications such as Li–ion batteries and Zn–air batteries [48–51]. Chen's group reported MOF-derived spinel-like Co-Mn-O nanotubes [52]. When it was employed as the cathode material in LOBs, a higher reversibility of 100 cycles was exhibited by curtailing capacity of 500 mAh/g at 0.16 mA/cm^2. The excellent electrochemical performance can be ascribed to the porous frameworks and the inherent catalytic activity in spinel oxides.

Liao's group co-loaded ruthenium and molybdenum trioxide in iron-doped ZIF-8 derived carbon (Ru-MoO_3/MDC) to obtain Li-O_2 cathode [53]. The cathodic catalyst combined the advantages of high specific surface area (derived from MDC), effective decomposition of discharge products (ascribed to Ru nanoparticles) and synergistic effect with MoO_3, leading to enhanced cyclability. The optimal electrode of Ru-MoO_3/MDC exhibited not only the highest initial discharge/charge capacity of 5343 mAh/g, but also the longest cycle life of 160 cycles at the current density of 100 mA/g with a cut-off capacity of 600 mAh/g. For comparison, pure MDC,

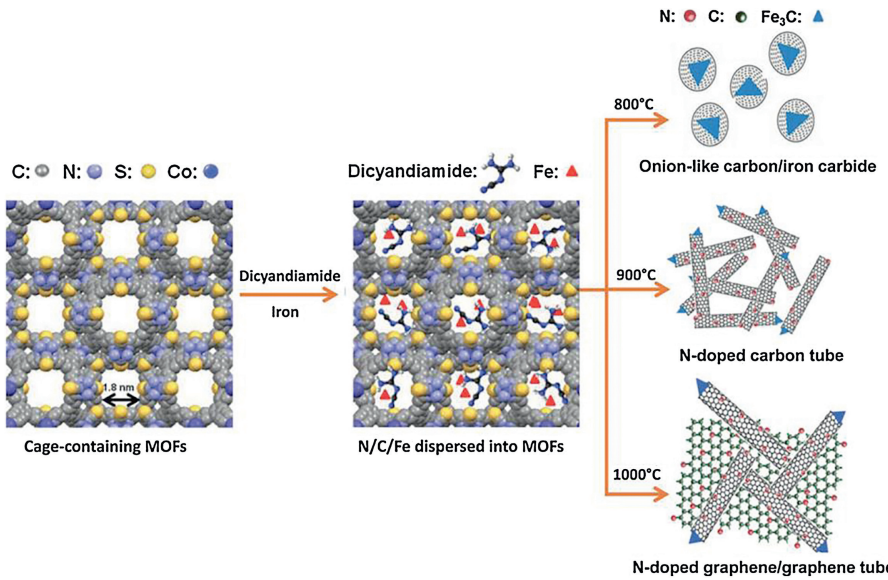

Fig. 6. Schematic illustration of formation of the carbon nanostructures found in the N-Fe-MOF catalysts synthesized at different heating temperatures. Reprinted with permission [54]. Copyright 2013, Wiley-VCH.

MDC with single Ru/MoO_3 (denoted as Ru/MDC and MoO_3/MDC) were investigated, respectively. Specifically, the effect of Ru and MoO_3 on the morphology of discharge products was revealed by *ex situ* SEM and discussed in each sample. Only "yo-yo-shaped" Ru-MoO_3/MDC with well-dispersed Li_2O_2 particles on the surface can decompose effectively.

3.3. MOF-derived carbides in Li–O_2 batteries

In a similar way, MOF-derived carbides are also effective catalysts of LOBs. The corresponding porous structures showed great potential in the cathode because of adequate exposure of active sites and plenty of metal sources.

Nitrogen-doped carbides usually exhibit high activity for ORR, which is the rate-determining step in LOBs. For the first time, Wu's group synthesized nitrogen-iron catalysts (denoted as N-Fe-MOF) derived from MOFs containing dicyandiamide (DCDA) and Fe species (Fig. 6) [54]. The obtained catalysts consist of Fe/Fe_3C nanoparticles with N-doped graphene. The best performer, N-Fe-MOF pyrolyzed at 1000 °C demonstrated high ORR activities in diverse pH conditions and the promoted cathodic performance in LOBs was owing to the catalytic activity of Fe_3C. Compared with other derivatives prepared under different temperature as well as other control samples including carbon black, Pt/C and MOF-free N-Fe, the optimized N-Fe-MOF showed the best result with onset potential around 3.1 V in the actual non-aqueous electrolyte (0.1 mol/L $LiPF_6$ in tetraethylene glycol dimethyl ether), approximating the theoretical potential of 3.1 V. Besides, the discharge capacity of N-Fe-MOF (~5300 mAh/g) is superior to other catalysts and it also shows higher average voltage plateau at 50 mA/g. Moreover, the N-Fe-MOF based cathode kept stable for 16 cycles and exhibited 27% capacity loss at a high current density of 400 mA/g until the 50^{th} cycles.

In order to find more facile fabricating approaches, 3D-porous graphene with Fe/Fe_3C (F-PNG) was established by the one-pot method and possessed abundant Fe nanocomposites [55]. The bifunctional catalyst raised discharge voltage plateau (2.91 V) and decreased charge voltage plateau (3.52 V).

Yan's group exploited molybdenum carbide as the cathode material in LOBs [56]. They reported N-doped α-MoC_{1-x} and β-Mo_2C nanocrystals derived from Mo-MOFs. The obtained catalysts own abundant homogeneously dispersed catalytic sites and porous structures that can accommodate plentiful discharge products. The 3D nano-meso-macro-architecture assists to obtain higher energy density and the nitrogen-doping improves the reduction rate of discharge products. Particularly, α-MoC_{1-x} oxygen electrode has a superior full discharge capacity of 20,212 mAh/g and stable cycling performance of 100 cycles at 200 mA/g with the limit-capacity of 1000 mAh/g. DFT result demonstrated that α-

Table 1
Noble metal, transition metal oxides, MOFs or MOF-derived materials for LOBs.

MOFs/other materials	Sample	Discharge capacity (mAh/g)	Charge potential (V)	Cycle number	ΔV	Ref.
Noble metal						
Ru	porous Ru	3720 (200 mA/g)	3.75 (200 mA/g)	>100 (200 mA/g)	1.0	[57]
Pt	CNF@Pt	6938 (200 mA/g)	~3.7 (500 mA/g)	163 (500 mA/g)	~1.0	[58]
Pd	Pd-NiO nanosheets	18900 (200 mA/g)	~3.3 (200 mA/g)	103 (200 mA/g)	0.5	[59]
Au	nanoporous Au	24000 (0.5 A/g)	~3.5 (2 A/g)	>140 (2 A/g)	~0.9	[60]
Pt-Au	Pt-Au NPs	21000 (50 mA/g)	3.6 (100 mA/g)	–	~1.0	[61]
Pt-Ir	Pt-Ir	2300 (0.05 mA/cm^2)	3.5 (0.05 mA/cm^2)	–	0.7	[62]
Transition metal oxides						
RuO_2	RuO_2 nanosheets	1110 (100 mA/g)	3.5 (100 mA/g)	>50 (200 mA/g)	0.69	[63]
MnO_2	3D α-MnO_2	8583 (100 mA/g)	~4.0 (200 mA/g)	170 (200 mA/g)	1.3	[64]
Co_3O_4	def-Co_3O_4-NS	~11000 (100 mA/g)	~3.7 (100 mA/g)	~150 (200 mA/g)	~1.1	[65]
Ti_4O_7	M-Ti_4O_7 nanospheres	3125 (100 mA/g)	4 (100 mA/g)	–	1.8	[66]
Pristine MOFs						
Mn-MOF-74	Mn-MOF-74	9420 (50 mA/g)	~4.4 (250 mA/g)	>30 (250 mA/g)	2	[19]
Co-MOF-74	Co-MOF-74-20	11350 (100 mA/g)	~3.9 (250 mA/g)	~8 (250 mA/g)	~1.2	[21]
MnCo-MOF-74	MnCo-MOF-74	11150 (200 mA/g)	~4.1 (200 mA/g)	44 (200 mA/g)	1.26	[23]
2D Mn-MOF	Mn-MOF nanosheets	9464 (100 mA/g)	~4.06 (100 mA/g)	>200 (100 mA/g)	1.28	[22]
Ni-MOF	Ni-MOF	9000 (0.12 mA/cm^2)	3.5 (0.12 mA/cm^2)	170 (0.6 mA/cm^2)	0.7	[20]
MOF-derived materials						
Co-MOF	3DP-NC-Co	1124 (0.05 mA/cm^2)	~4.1 (0.1 mA/cm^2)	~160 h (0.1 mA/cm^2)	~1.4	[32]
Ru-MOF	Ru-MOF-C	–	~3.8 (500 mA/g)	>800 (500 mA/g)	~1	[33]
FeCo-MOF	MOF(Fe/Co)-CNTs-600	>5000 (100 mA/g)	~4.0 (100 mA/g)	40 (100 mA/g)	~1.5	[38]
ZIF-9	Co_3O_4/carbon nanofiber	760 (500 mA/g)	~4.1 (500 mA/g)	–	1.7	[40]
ZIF-8@ZIF-67	GPC-Co_3O_4	1575 (125 mA/g)	~3.5 (125 mA/g)	>50 (250 mA/g)	0.84	[39]
ZIF-67	Wood-D/Co_3O_4/C	120 (0.1 mA/cm^2)	~4.2 (1.0 mA/cm^2)	>380 (1.0 mA/cm^2)	1.5	[41]
ZIF-9	Co-CoO@NC	5582 (0.05 mA/cm^2)	~3.9 (0.05 mA/cm^2)	>42 (0.1 mA/cm^2)	1.3	[42]
PAN@ZIF-67	CNFs@Co-CoO	~3500 (200 mA/g)	~4.2 (200 mA/g)	38 (200 mA/g)	~1.7	[43]
Co-MOF	Co/CoO/C@Ni	8000 (0.1 mA/cm^2)	~4.0 (0.1 mA/cm^2)	70 (0.1 mA/cm^2)	~1.1	[44]
MIL-100(Fe)	γ-Fe_2O_3/carbon	5970 (0.1 mA/cm^2)	~3.75 (0.1 mA/cm^2)	>30 (0.1 mA/cm^2)	~1.05	[45]
MIL-101(Cr)	Cr_2O_3@OPC	~4800 (0.1 mA/cm^2)	~3.7 (0.1 mA/cm^2)	>50 (0.1 mA/cm^2)	~1.0	[46]
Fe(III)-MOF-5	ZnO/$ZnFe_2O_4$/C	>11,000 (300 mA/g)	4.0 (300 mA/g)	15 (300 mA/g)	1.3	[47]
$Mn_3[Co(CN)_6]_2{\cdot}9H_2O$	Co-Mn-O nanocubes	7653 (0.04 mA/cm^2)	~4.1 (0.16 mA/cm^2)	100 (0.16 mA/cm^2)	1.31	[52]
iron-doped ZIF-8	Ru-MoO_3/MDC	5343 (100 mA/g)	4.2 (100 mA/g)	>160 (100 mA/g)	~1.8	[53]
Co-MOF	N-Fe-MOF	5300 (50 mA/g)	3.8 (50 mA/g)	~50 (400 mA/g)	1	[54]
MIL-100(Fe)	F-PNG	7150 (0.1 mA/cm^2)	~3.9 (0.1 mA/cm^2)	~30 (0.1 mA/cm^2)	~1.25	[55]
$[H_2im]_4[Mo_8O_{26}(Him)_2]$	α-MoC_{1-x}	20,212 (200 mA/g)	3.95 (100 mA/g)	~100 (200 mA/g)	~1.4	[56]
ZIF-67	BND-Co@G-MCHs	5.98 mAh/cm^2 (0.1 mA/cm^2)	~3.7 (0.1 mA/cm^2)	~30 (0.1 mA/cm^2)	~0.95	[67]
ZIF-67	Co_9S_8@CPNs	7000 (50 mA/g)	~4.0 (100 mA/g)	~110 (100 mA/g)	~1.4	[68]
ZIF-8/GO	NPC-rGO	>12,000 (50 mA/g)	~4.0 (200 mA/g)	>125 (200 mA/g)	~1.4	[69]

MoC_{1-x} was the best performer due to shorter charge transfer routes and better O_2 adsorption capability.

3.4. Other MOF-derived materials in Li–O_2 batteries

In addition to MOF-derived metal, metal oxides and carbides, many other MOF derivatives have shown excellent performance in LOBs. Exciting results were presented and compared with some different materials in Table 1 [57–66].

MOF-derived nitrides are another kind of effective ORR catalyst. Amine's group designed novel capsules of nitrogen-doped Co wrapped with graphene [67]. The unique morphology of BND-Co@G-MCH was fabricated in two steps: thermal treatment in argon first and then in mixed gas of 70% NH_3 and 30% N_2. The final products consist of biphasic N-doped heterostructural cobalt nitride incorporating few layers of N-doped graphene. Besides, the uniform multiple-capsule morphology provided sufficient room for accommodation of discharge products and plentiful surface for gas diffusion which can boost electrical conductivity and catalytic activity at the same time. The cyclic performance of the carbon fiber electrode ran 30 cycles limited by lithium anode. When reassembled the original cathode with fresh lithium metal, it can operate for an extra 30 cycles. Indeed, the double mass of BND-Co@G-MCH loading on flexible substract (Ni foam), showed higher discharge capacity than carbon-fiber electrode. Furthermore, according to the DFT calculation result (Fig. 7), the N-doped defects in graphene and the exposed CoN surface have stronger interaction with the discharge product of disc-type Li_2O_2 in contrast to the pristine graphene.

Beyond that, sulfides were also developed as catalysts in LOBs. Peng's group synthesized Co_9S_8@carbon derived from ZIF-67 [68]. The carbon nanocages, as the multifunctional catalyst in ORR and OER, achieved higher energy density of 72.2%, lower overpotential of 1.057 V in initial discharge-charge cycle and longer cycle life of 110 cycles at 100 mA/g than that of Super P electrode. Moreover, DFT calculation elucidated the formation process of discharge products. Co_9S_8@carbon porous nanocages were proved high catalytic activity and improved cycle life by preventing the formation of Li_2CO_3.

Metal-free carbon porous materials also play an important role. Bu's group combined self-inherent structural ZIF-8 derivative with reduced graphene oxide (rGO) as the cathode in LOBs [69]. By evaporating Zn at 1000 °C in N_2 atmosphere, nitrogen-doped porous carbon/rGO was synthesized. The mesopores and N-doping structure provided plentiful active sites that promoted the reversibility. NPC/rGO displayed superior initial discharge capacity of ~7500 mAh/g and high Coulombic efficiency of 90.1% at 200 mA/g compared with the parent NPC and rGO. Moreover, at the current density of 50 mA/g, the specific capacity of NPC/rGO is over 12,000 mAh/g with coulombic efficiency of 93.2%. With a capacity limitation of 1000 mAh/g at 200 mA/g, it still maintained stable during 125 cycles.

3.5. MOF-derived materials in Li–CO_2 batteries

In order to realize a high-efficient decomposition of Li_2CO_3, our group designed highly dispersed N-doped carbon-coated Mn skeleton combining 2D graphene nanosheet (MnO@NC-G) derived from MET-2, a Mn-based MOF $Mn(C_2H_2N_3)_2$ ($C_2H_2N_3$ = 1*H*-1,2,3-triazole) (Fig. 8) [70]. The porous nanocatalyst combining monodispersed MnO with N-doped carbon displayed high catalytic activities, sufficient electronic transportation pathway and wide-range hierarchical porous sites. Consequently, the MnO@NC-G based electrode promoted the cathode performance: (1) lower ΔV (0.88 V) with high coulombic efficiency of 95.6% and ultrahigh discharge capacity of 25,021 mA/g were achieved at 50 mA/g; (2) extremely high rate capability was recorded up to 1 A/g compared to most gaseous cathode (< 400 mA/g) in Li−CO_2 system; (3) superior reversibility was shown at high current density. The active sample displayed more than 10 cycle life with a capacity limit of 5000 mAh/g at 400 mA/g as well as 206 cycles at high current density of 1 A/g with a limited capacity of 1000 mAh/g. Remarkably, the cathode was reassembled with fresh lithium anode and achieved 176 cycles more. These results provided a new strategy to synthesize highly efficient electrocatalysts for practical LABs.

Above all, MOFs are favorable templates for fabricating homogenously dispersed metal and metal oxide/carbon compounds. To further enhance energy density and empower practical applications of LABs, it is essential to construct 3D conducting network with large specific surface area to accommodate discharge products.

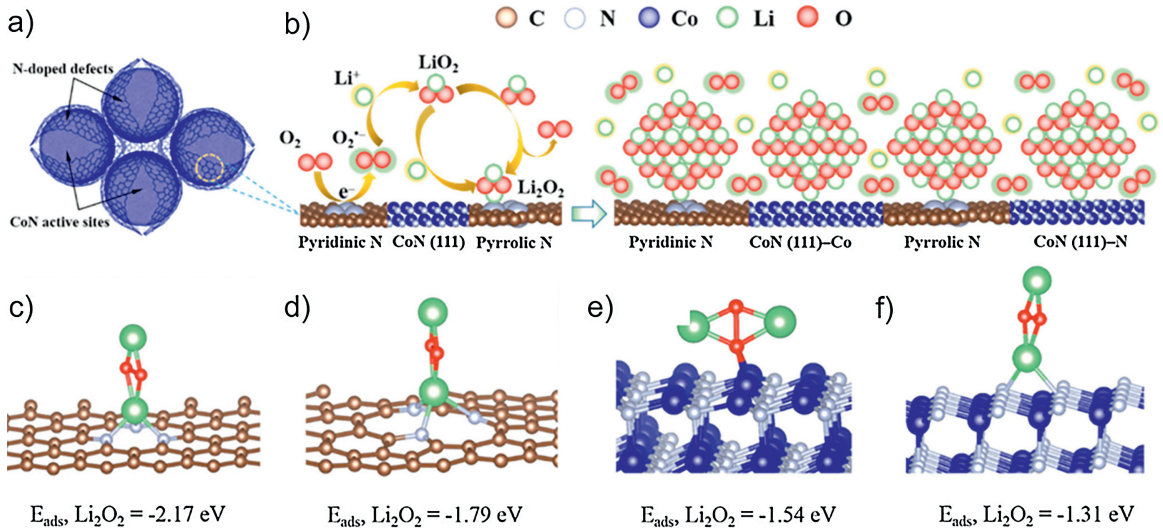

Fig. 7. Density functional calculations and electrochemical mechanism study of BND-Co@G-MCH. (a) Schematic of the biphasic N-doped cobalt@graphene multiple- capsule heterostructures. (b) Schematic of the proposed mechanism for reactions occurring during the discharge process. (c–f) Density functional theory (DFT) calculations showing the binding energies between Li_2O_2 monomer and active sites on the support catalyst surfaces. The pyridinic (c) and pyrrolic (d) N-doping sites on graphenes, and the CoN (111) surface with the Co (e) and N (f) terminations were taken into account for calculations. Reprinted with permission [67]. Copyright 2017, American Chemical Society.

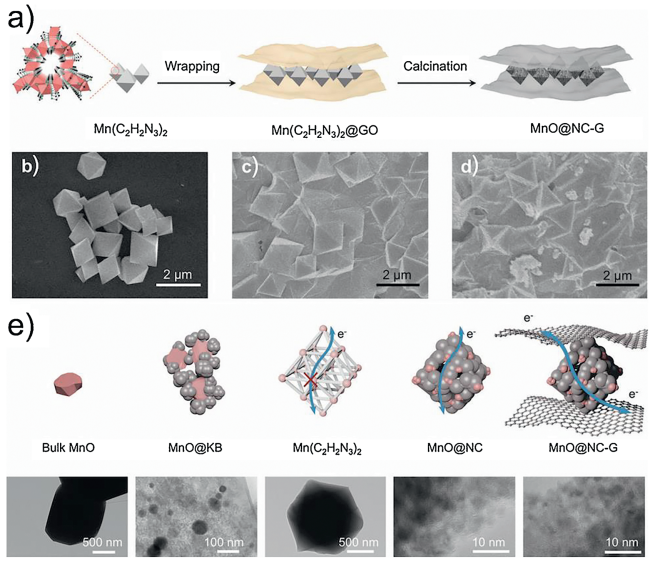

Fig. 8. (a) Synthetic route of MnO@NC-G. SEM images of (b) $Mn(C_2H_2N_3)_2$ particles, (c) $Mn(C_2H_2N_3)_2$ wrapped with GO and (d) MnO@NC-G. (e) Schematic illustration of the structural features of different Mn(II) catalysts for Li-CO_2 batteries and their corresponding TEM images. Reprinted with permission [70]. Copyright 2019, The Royal Society of Chemistry.

4. Conclusions and perspectives

In this review, we have summarized the encouraging advancements of pristine MOFs and MOFs-derived materials in LABs during the past 5 years. MOFs and their derivatives, which hold high specific surface area, designable skeleton and abundant catalytic sites, have exhibited the possibility in LABs.

Although many achievements have been achieved, there are still enormous challenges in LABs. In our opinion, future works could be focused on the following two aspects:

(1) Cathode: MOFs have been widely utilized to obtain outstanding cathodic performance. However, the electronic conductivity of MOFs is still insufficient. And the catalytic efficiency of the cathode should be further improved to fulfill the increasing demand. In our view, the following three aspects deserve more attention: a) mixed metallic MOFs usually exhibit synergistic effect leading to higher catalytic activity; b) conductive MOFs could solve the problem of poor electrical conductivity; c) MOF-derived single-atom catalysts could be a new class of promising MOF-based materials in LABs cause of their excellent activities in ORR [71–73].

(2) Separator: It is still a very infant stage for MOF-based separator. The controllable porosity of MOFs can inhibit the diffusion of gas and mediators to Li anode side. Hence the degradation of lithium could be reduced and the lifespan of LABs could be promoted [74,75]. Therefore, the rational design of pore and channels in MOFs is essential, besides, the stability of MOFs could be enhanced to sustain long cycling performances.

In conclusion, with the emerging of more and more MOFs and the corresponding derivatives with novel structures and various compositions, the potential of MOFs is tremendous. Undoubtedly, MOFs are promising to play an important role in enhancing the comprehensive performance of LABs in the future.

Acknowledgments

This work was financially supported by the National Natural Science Foundation of China (Nos. 21625102, 21471018), the Beijing Municipal Science and Technology Project (No. Z181100004418001) and the Beijing Institute of Technology Research Fund Program.

References

[1] F. Cheng, J. Chen, Chem. Soc. Rev. 41 (2012) 2172–2192.
[2] J.S. Lee, S. Tai Kim, R. Cao, et al., Adv. Energy Mater. 1 (2011) 34–50.
[3] Q. Liu, Z. Chang, Z. Li, et al., Small Methods 2 (2018) 1700231.
[4] D. Larcher, J.M. Tarascon, Nat. Chem. 7 (2015) 19–29.
[5] P.G. Bruce, S.A. Freunberger, L.J. Hardwick, et al., Nat. Mater. 11 (2011) 19–29.
[6] D. Aurbach, B.D. McCloskey, L.F. Nazar, et al., Nat. Energy 1 (2016) 16128.
[7] M. Asadi, B. Sayahpour, P. Abbasi, et al., Nature 555 (2018) 502–506.
[8] G. Girishkumar, B. McCloskey, A.C. Luntz, et al., J. Phys. Chem. Lett. 1 (2010) 2193–2203.
[9] H. Furukawa, K.E. Cordova, M. O'Keeffe, et al., Science 341 (2013) 1230444.
[10] J.R. Li, R.J. Kuppler, H.C. Zhou, Chem. Soc. Rev. 38 (2009) 1477–1504.
[11] J.R. Li, Y. Ma, M.C. McCarthy, et al., Coord. Chem. Rev. 255 (2011) 1791–1823.
[12] D. Farrusseng, S. Aguado, C. Pinel, Angew. Chem. 48 (2009) 7502–7513.
[13] D.M. D'Alessandro, B. Smit, J.R. Long, Angew. Chem. 49 (2010) 6058–6082.
[14] A. Corma, H. Garci'a, F.X. Llabre's i Xamena, Chem. Rev. 110 (2010) 4606–4655.
[15] L. Wang, Y. Han, X. Feng, et al., Coord. Chem. Rev. 307 (2016) 361–381.
[16] X. Zhang, A. Chen, M. Zhong, et al., Electrochem. Energy Rev. 2 (2018) 29–104.
[17] R. Zhao, Z. Liang, R. Zou, et al., Joule 2 (2018) 2235–2259.
[18] J. Zhou, B. Wang, Chem. Soc. Rev. 46 (2017) 6927–6945.
[19] D. Wu, Z. Guo, X. Yin, et al., Adv. Mater. 26 (2014) 3258–3262.
[20] X. Hu, Z. Zhu, F. Cheng, et al., Nanoscale 7 (2015) 11833–11840.
[21] W. Yan, Z. Guo, H. Xu, et al., Mater. Chem. Front. 1 (2017) 1324–1330.
[22] M. Yuan, R. Wang, W. Fu, et al., ACS Appl. Mater. Interfaces 11 (2019) 11403–11413.
[23] S.H. Kim, Y.J. Lee, D.H. Kim, et al., ACS Appl. Mater. Interfaces 10 (2017) 660–667.
[24] Y. Qiao, Y. He, S. Wu, et al., ACS Energy Lett. 3 (2018) 463–468.
[25] L. Cao, F. Lv, Y. Liu, et al., Chem. Commun. 51 (2015) 4364–4367.
[26] K. Takechi, T. Shiga, T. Asaoka, Chem. Commun. 47 (2011) 3463–3465.
[27] L. Qie, Y. Lin, J.W. Connell, et al., Angew. Chem. 56 (2017) 6970–6974.
[28] F. Cai, Z. Hu, S.-L. Chou, Adv. Sustain. Syst. 2 (2018) 1800060.
[29] S. Xu, S.K. Das, L.A. Archer, RSC Adv. 3 (2013) 6656–6660.
[30] Z. Zhao, J. Huang, Z. Peng, Angew. Chem. 57 (2018) 3874–3886.
[31] S. Li, Y. Dong, J. Zhou, et al., Energy Environ. Sci. 11 (2018) 1318–1325.
[32] Z. Lyu, G.J.H. Lim, R. Guo, et al., Adv. Funct. Mater. 29 (2019) 1806658.
[33] X. Meng, K. Liao, J. Dai, et al., ACS Appl. Mater. Interfaces 11 (2019) 20091–20097.
[34] X.F. Lu, L.F. Gu, J.W. Wang, et al., Adv. Mater. 29 (2017) 1604437.
[35] L. Yan, L. Cao, P. Dai, et al., Adv. Funct. Mater. 27 (2017) 1703455.
[36] B. You, N. Jiang, M. Sheng, et al., ACS Catal. 5 (2015) 7068–7076.
[37] S. Zhao, Y. Wang, J. Dong, et al., Nat. Energy 1 (2016) 16184.
[38] H. Wang, F. Yin, P. Lv, et al., Int. J. Hydrogen Energy 42 (2017) 2127–2133.
[39] J. Tang, S. Wu, T. Wang, et al., ACS Appl. Mater. Interfaces 8 (2016) 2796–2804.
[40] M.J. Song, I.T. Kim, Y.B. Kim, et al., Electrochim. Acta 182 (2015) 289–296.
[41] G. Zhao, Y. Liu, L. Tang, et al., ACS Appl. Energy Mater. 2 (2019) 2113–2121.
[42] X. Chen, C. Chen, X. Zhang, et al., ChemistrySelect 3 (2018) 9276–9283.
[43] A. Li, X. Zhang, Z. Xie, et al., Inorg. Chem. 57 (2018) 14476–14479.
[44] C. Hua, Z. Qian, M. Chen, et al., J. Alloys Compd. 749 (2018) 378–384.
[45] W. Chen, Z. Zhang, W. Bao, et al., Electrochim. Acta 134 (2014) 293–301.
[46] Y. Gan, Y. Lai, Z. Zhang, et al., J. Alloys. Compd. 665 (2016) 365–372.
[47] W. Yin, Y. Shen, F. Zou, et al., ACS Appl. Mater. Interfaces 7 (2015) 4947–4954.
[48] Y. Kang, D. Zou, J. Zhang, et al., Electrochim. Acta 244 (2017) 222–229.
[49] Y. Ma, C.W. Tai, R. Younesi, et al., Chem. Mater. 27 (2015) 7698–7709.
[50] M. Prabu, P. Ramakrishnan, H. Nara, et al., ACS Appl. Mater. Interfaces 6 (2014) 16545–16555.
[51] L. Zhou, D. Zhao, X.W. Lou, Adv. Mater. 24 (2012) 745–748.
[52] J. Zhang, L. Wang, L. Xu, et al., Nanoscale 7 (2015) 720–726.
[53] J. Li, Y. Deng, L. Leng, et al., ACS Sustain. Chem. Eng. 7 (2018) 2296–2303.
[54] Q. Li, P. Xu, W. Gao, et al., Adv. Mater. 26 (2014) 1378–1386.
[55] Y. Lai, W. Chen, Z. Zhang, et al., Electrochim. Acta 191 (2016) 733–742.
[56] H. Yu, K.N. Dinh, Y. Sun, et al., Nanoscale 10 (2018) 14877–14884.
[57] K. Liao, T. Zhang, Y. Wang, et al., ChemSusChem 8 (2015) 1429–1434.
[58] H.T. Bui, D.Y. Kim, D.W. Kim, et al., Carbon 130 (2018) 94–104.
[59] F.L. Meng, Z.W. Chang, J.J. Xu, et al., Mater. Horiz. 5 (2018) 298–302.
[60] X. Guo, J. Han, P. Liu, et al., Sci. Rep. 6 (2016) 33466.
[61] Y.C. Lu, Z. Xu, H.A. Gasteiger, et al., J. Am. Chem. Soc. 132 (2010) 12170–12171.
[62] F.S. Ke, B.C. Solomon, S.G. Ma, et al., Electrochim. Acta 85 (2012) 444–449.
[63] K. Liao, X. Wang, Y. Sun, et al., Energy Environ. Sci. 8 (2015) 1992–1997.
[64] R. Bi, G. Liu, C. Zeng, et al., Small 15 (2019) e1804958.
[65] R. Gao, Z. Shang, L. Zheng, et al., Inorg. Chem. 58 (2019) 4989–4996.
[66] S. Lee, G.H. Lee, J.C. Kim, et al., ACS Catal. 8 (2018) 2601–2610.
[67] G. Tan, L. Chong, R. Amine, et al., Nano Lett. 17 (2017) 2959–2966.
[68] Y. Dou, R. Lian, Y. Zhang, et al., J. Mater. Chem. A 6 (2018) 8595–8603.
[69] M. Zhong, X. Zhang, D.H. Yang, et al., Inorg. Chem. Front. 4 (2017) 1533–1538.
[70] S. Li, Y. Liu, J. Zhou, et al., Energy Environ. Sci. 12 (2019) 1046–1054.
[71] L. Jiao, H.L. Jiang, Chemistry 5 (2019) 786–804.
[72] Y. Chen, S. Ji, C. Chen, et al., Joule 2 (2018) 1242–1264.
[73] J. Wang, W. Liu, G. Luo, et al., Energy Environ. Sci. 11 (2018) 3375–3379.
[74] L. Liu, C. Du, S. Wang, et al., Chin. Chem. Lett. 29 (2018) 1781–1784.
[75] Z. Jiang, T. Liu, L. Yan, et al., Energy Storage Mater. 11 (2018) 267–273.